Capture and fission analysis of various superheavy isotopes with A_{CN} = 258–280

Gurjit Kaur[1] **and Manoj K Sharma**

School of Physics and Materials Science, Thapar Institute of Engineering and Technology,
Patiala—147004, Punjab, India

E-mail: gurjitsaini2505@gmail.com and msharma@thapar.edu

CrossMark

Abstract

The capture and fission analysis of heavy ion induced fusion reactions leading to the formation of $Z = 107$–111 superheavy nuclei has been carried out. Attempts have been made to analyze the synthesis traits, such as excitation functions, formation probabilities, barrier characteristics etc. The ℓ-summed Wong model provides a decent description of available data on capture (σ_{Cap}) and fusion-fission (σ_{ff}) cross-sections and hence is exploited to make relevant predictions for future experiments. The capture and fusion-fission excitation functions are predicted for the least explored region of superheavy nuclei (SHN) i.e. $Z = 107$–111. The role of mass-asymmetry (η), Coulomb factor ($Z_P Z_T$), deformation and orientations, Businari-Gallone mass-asymmetry (α_{BG}), fission barrier (B_f) etc is duly explored. The present study concludes that the mass-asymmetric reactions involving ^{24}Mg, ^{30}Si, and ^{36}S projectiles are preferred for the synthesis of unknown isotopes of $Z = 107$–111. Alternatively, the doubly magic ^{48}Ca-projectile also provides a competing alternative to produce neutron-rich isotopes of the above-mentioned SHN.

1. Introduction

The fusion of two colliding nuclei is a fundamental phenomenon, though there are various dynamical aspects that are not fully explored. The development of intensive beam currents and sensitive detection methods have enabled us to synthesize and study the nuclei in the unexplored region of the nuclear chart. Numerous reactions and recognition techniques have been applied in the past to scrutinize transuranic elements. The most successful methods have been the fusion evaporation reactions of already known elements, recoil-separation techniques, identification through detectors *etc.* Such techniques are constantly further refined and employed for the exploration of nuclear properties of new elements. The cold fusion reactions (^{208}Pb, ^{209}Bi + massive projectile (A_P > 50)) have been used since 1974 for the synthesis of elements with $Z = 107$–112 [1–3]. Unfortunately, the forecasts for cold fusion reactions are not optimistic because of

increased fusion hindrance and small neutron excess. Within the last two decades, researchers successfully synthesized six new superheavy elements with $Z = 113$–118 by following a different approach in which the high intensity beam of ^{48}Ca projectile is aimed at actinide targets [4–6]. Instead of this, the mass-asymmetric reactions of actinide nuclei with lighter projectiles like magnesium (Mg) to potassium (K) are also of great interest to fill the gap between hot and cold fusion reactions.

Several experiments were performed for the cold synthesis of $Z = 107$–112 superheavy nuclei. The $Z = 107$ superheavy system was produced in ^{209}Bi(^{54}Cr,1n-2n)$^{261-262}$Bh and ^{208}Pb(^{55}Mn,1n-2n)$^{261-262}$Bh [7] reactions pairs and ^{208}Pb(^{58}Fe,1n)^{265}Hs [8] report the synthesis of $Z = 108$. Additionally, the pair reactions ^{209}Bi(^{58}Fe,1n)^{266}Mt and ^{208}Pb(^{59}Co,1n)^{266}Mt [9] were investigated for the production of $Z = 109$. The experiments involving the synthesis of elements $Z = 110$, 111, and 112 use respectively, ^{208}Pb(^{64}Ni,1n)^{271}Ds, ^{209}Bi(^{64}Ni,1n)^{272}Rg; ^{208}Pb(^{65}Cu,1n)^{272}Rg, and ^{208}Pb(^{70}Zn,1n)^{277}Cn [10–12]. The long lived isotopes of

---

superheavy elements (SHE) produced in the experiments are still neutron deficient. The short lifetime and low production cross-sections have posed difficulties in studying the various properties of superheavy elements. Therefore, the quest for suitable target-projectile combinations for the synthesis of stable superheavy elements is still going on. For the purpose, one can use the actinide targets with stable projectile lighter than ^{48}Ca to produce some unknown neutron deficient isotopes with high efficiency. Some of the aforementioned elements were also synthesized using the types of reaction choices like ^{248}Cm(^{26}Mg,5n-3n)$^{269-271}$Hs [13], ^{238}U(^{36}S,5n-3n)$^{269-271}$Hs [14], ^{226}Ra(^{48}Ca,4n)^{270}Hs [15], and ^{238}U(^{48}Ca,4n-3n)$^{282-283}$Cn [5]. The idea of using a more asymmetric reaction pair reduces the suppression of fusion and hence results in higher compound nuclear formation cross-sections. Hence it will be of interest to explore the peculiarities of different target-projectile (t-p) combinations for the synthesis of elements like $Z = 107$, 109, 110, and 111 already synthesized in cold fusion reactions.

The sensibility of colliding partners of a reaction leading to the formation of superheavy nuclei play significant role even at energies close to the barrier. The synthesis cross-sections of these nuclei are very small. Hence, the precise calculations and predictions of cross-sections are very important so that experimentalists are able to select the best target-projectile (t-p) combinations as well as required energy for the feasibility of superheavy nuclei. In this article, the main concern is on the coalescence of unknown superheavy isotopes with charge number $Z = 107$–111. For this purpose, different actinide-based hot fusion reactions with light, medium, and heavy t-p combinations are considered. Firstly, the available experimental data is addressed for reliable predictions of capture (σ_{capture}) and fusion (σ_{fusion}) excitation functions. For light and medium nuclei, the fission barrier (B_f) is high and compound nucleus formation probability (P_{CN}) is close to unity i.e. $P_{\text{CN}} \approx 1$ and hence $\sigma_{\text{capture}} \approx \sigma_{\text{fusion}} \approx \sigma_{\text{ER}}$ [16–18]. But for heavy/superheavy systems, the scenario is different and non-compound nucleus (nCN) (or quasi-fission (QF)) processes and fusion-fission channels substantially determine the whole dynamics. The $P_{\text{CN}} < 1$, which leads to $\sigma_{\text{capture}} = \sigma_{\text{fusion}} + \sigma_{\text{QF}}$. Further, the contribution of evaporation residues (ERs) to fusion is very small (nb or pb order) and fusion-fission (ff) processes dominate, so $\sigma_{\text{fusion}} \approx \sigma_{\text{ff}}$ [19–21].

As the evaporation residue study of some isotopes of $Z = 107$–111 is already done in [22], the main interest of the present work is to study the following: (i) to predict the capture and fusion-fission excitation functions for unknown superheavy nuclei with $Z = 107$–111 in hot fusion reactions; (ii) the competition between quasi-fission and fusion-fission events is explored in terms of mass-asymmetry (η), Coulomb factor (Z_1Z_2), Businaro-Gallone mass-asymmetry point (α_{BG}) etc; (iii) the determination of compound nucleus formation probability (P_{CN}); (iv) the effect of deformations and orientations on the fusion mechanism.

In view of the above, the paper is organized as follows: section 2 gives a brief overview of the methodology (ℓ-summed Wong model). Subsequent to this, the details of calculations and the results are discussed in section 3. Finally, the summary and conclusions are presented in section 4.

2. Methdology

2.1. The potential

The total interaction potential for two colliding nuclei is calculated by adding the repulsive Coulomb term (V_C), centrifugal potential (V_ℓ), and nuclear potential (V_N). Numerous efforts have been straggled to determine the exact behavior of inter nuclear potential [23–28] and the proximity potentials have been employed with resealable success [27, 28]. The total interaction potential is the function of radial distance (R) between two nuclei, collision angle (θ), deformation parameter (β_i), temperature (T) and is given by

$$V_T^\ell(R, \theta_i) = V_C(R, Z_i, \beta_{\lambda i}, \theta_i, T) + V_P(R, A_i, \beta_{\lambda i}, \theta_i, T) \\ + V_\ell(R, A_i, \beta_{\lambda i}, \theta_i, T). \tag{1}$$

The nuclear proximity potential [27, 28] for deformed, orientated nuclei is given by

$$V_N(s_0(T)) = 4\pi \bar{R} \gamma b(T) \Phi(s_0(T)) \tag{2}$$

where $b(T) = 0.99(1 + 0.009T^2)$ is the nuclear surface thickness, γ is the surface energy constant and $\bar{R}(T)$ is the mean curvature radius. Φ is a universal function which is independent of the shapes of nuclei or the geometry of the nuclear system but depends on minimum separation distance $s_0(T)$ [27].

The Coulomb potential for a multipole-multipole interactions and two non-overlapping charge distributions [29, 30] is defined as

$$V_C(R, Z_i, \beta_{\lambda i}, \theta_i, T) = \frac{Z_1 Z_2 e^2}{R} + 3Z_1 Z_2 e^2 \\ \times \sum_{\lambda, i=1,2} \frac{R_i^\lambda(\alpha_i)}{(2\lambda + 1)R^{\lambda+1}} \\ \times Y_\lambda^{(0)}(\theta_i) \left[\beta_{\lambda i} + \frac{4}{7} \beta_{\lambda i}^2 Y_\lambda^{(0)}(\theta_i) \right]. \tag{3}$$

The centrifugal potential of the nuclei is given by

$$V_\ell(R, A_i, \beta_{\lambda i}, \theta_i, T) = \frac{\hbar^2 \ell(\ell + 1)}{2I} \tag{4}$$

where ℓ is angular momentum and $I = I_S = \mu R^2 + \frac{2}{5}A_1 m R_1^2(\alpha_1, T) + \frac{2}{5}A_2 m R_2^2(\alpha_2, T)$ is the moment of inertia.

2.2. Capture or total cross-sections

The capture cross-section, in terms of angular-momentum (ℓ) partial waves, for two deformed and oriented nuclei (with orientation angles θ_i), lying in the same planes and colliding with center-of-mass energy $E_{\text{c.m.}}$, is

$$\sigma_{\text{cap}}(E_{\text{c.m.}}, \theta_i) = \sum_{\ell=0}^{\infty} \sigma_\ell = \frac{\pi}{k^2} \sum_{\ell=0}^{\infty} (2\ell + 1) P_\ell \tag{5}$$

with $k = \sqrt{\frac{2\mu E_{\text{c.m.}}}{\hbar^2}}$ and μ is the reduced mass, P_ℓ is the transmission coefficient for each ℓ, which describes the penetrability across the barrier.

The penetrability P_ℓ, used in equation (5), is defined as

$$P_\ell = \left[1 + \exp\left(\frac{2\pi(V_B^\ell - E_{\text{c.m.}})}{\hbar\omega_\ell}\right)\right]^{-1}. \tag{6}$$

In equation (6), Hill Wheeler approximation [31] is applied to calculate the penetrability. In such an approximation, the dependance of transmission probability is worked out in terms of fusion barrier height V_B^ℓ and curvature $\hbar\omega_\ell(E_{\text{c.m.}}, \theta_i)$. There are alternative methods such as the Wentzel-Kramers-Brillouin (WKB) method [32] where the integration over the whole barrier is taken. In the recent past, one of us and collaborators have made a comparison of both the approximations, i.e. Hill Wheeler and WKB in [33] and found that either of the two methods may be applied for the addressal of fusion cross-sections. In penetrability expression, $\hbar\omega_\ell$ is evaluated at the barrier position $R = R_B^\ell$ corresponding to barrier height V_B^ℓ and is given as

$$\hbar\omega_\ell(E_{\text{c.m.}}, \theta_i) = \hbar\left[|\mathrm{d}^2V_T^\ell(R)/\mathrm{d}R^2|_{R=R_B^\ell}/\mu\right]^{1/2} \tag{7}$$

with R_B^ℓ obtained from the condition $|\mathrm{d}V_T^\ell(R)/\mathrm{d}R|_{R=R_B^\ell} = 0$. Instead of solving equation (5) explicitly, which requires the complete ℓ-dependent potentials $V_T^\ell(R, E_{\text{c.m.}}, \theta_i)$, Wong [29] carried out the ℓ-summation approximately under specific conditions:(i) $\hbar\omega_\ell \approx \hbar\omega_0$ and (ii)$V_B^\ell \approx V_B^0 + \frac{\hbar^2\ell(\ell+1)}{2\mu R_B^0 2}$, which means to assume $R_B^\ell \approx R_B^0$ also. Using these approximations and replacing the ℓ summation in equation (5) by an integral gives the $\ell = 0$ barrier-based Wong formula

$$\sigma_{\text{Cap}}(E_{\text{c.m.}}, \theta_i) = \frac{R_B^{02}\hbar\omega_0}{2E_{\text{c.m.}}}\ln\left\{1 + \exp\left[\frac{2\pi}{\hbar\omega_0}(E_{\text{c.m.}} - V_B^0)\right]\right\}. \tag{8}$$

The barrier radius (R_B) for $\ell = 0$ is obtained from condition

$$\left|\frac{\mathrm{d}V_T(R)}{\mathrm{d}R}\right|_{R=R_B} = 0. \tag{9}$$

The curvature $\hbar\omega_0(E_{\text{c.m.}}, \theta_i)$, calculated at the barrier position $R = R_B^0$ corresponding to the maximum barrier height $V_B^0(E_{\text{c.m.}}, \theta_i)$, is given as

$$\hbar\omega_0(E_{\text{c.m.}}, \theta_i) = \hbar\left[|\mathrm{d}^2V^0(R)/\mathrm{d}R^2|_{R=R_B^0}/\mu\right]^{1/2}. \tag{10}$$

In equation (5), $\sigma_{\text{Cap}}(E_{\text{c.m.}}, \theta_i)$ is calculated for each orientation and then integrated over angle θ_i (i = 1, 2) to give the final capture cross-section as

$$\sigma_{\text{Cap}}(E_{\text{c.m.}}) = \int_{\theta_i=0}^{\pi/2} \sigma(E_{\text{c.m.}}, \theta_i)\sin\theta_1\mathrm{d}\theta_1\sin\theta_2\mathrm{d}\theta_2. \tag{11}$$

Recently, Kumar and collaborators [34] carried out the extension of the Wong formula known as the ℓ-summed extended Wong formula. The extended version includes ℓ summation up to ℓ_{max}, given as

$$\sigma_{\text{cap}}(E_{\text{c.m.}}, \theta_i) = \frac{\pi}{k^2}\sum_{\ell=0}^{\ell_{\text{max}}}(2\ell + 1)P_\ell. \tag{12}$$

The maximum possible angular momentum (ℓ_{max}) of a system at a given energy is calculated using relation [35]

$$\ell_{\text{max}} = \frac{R_a\sqrt{2\mu[E_{\text{c.m.}} - V(R_a, \ell = 0)]}}{\hbar} \tag{13}$$

2.3. Fusion cross-sections

The fusion for superheavy nuclei constitute only a part to the capture events, so the fusion cross-section is always equal to or less than the capture cross-section and is expressed as

$$\sigma_{\text{fusion}}(E_{\text{c.m.}}, \theta_i) = \frac{\pi}{k^2}\sum_{\ell=0}^{\infty}(2\ell + 1)P_\ell P_{\text{CN}}. \tag{14}$$

2.4. Compound nucleus formation probability (P_{CN})

In above equation, P_{CN} is the compound nucleus formation probability. The mean fissility parameter (x_m) dependent formation probability (P_{CN}) is defined as the linear combination of the effective fissility parameter x_{eff} and compound nucleus fissility parameter x_{CN}. The mean fissility parameter is defined as [36]

$$x_{\text{m}} = 0.75x_{\text{eff}} + 0.25x_{\text{CN}}. \tag{15}$$

The compound nucleus fissility parameter x_{CN} is the ratio of competing Coulomb and nuclear forces for compact shapes and is given by [37]

$$x_{\text{CN}} = \frac{(Z^2/A)}{(Z^2/A)_{\text{crit}}} = \frac{(Z^2/A)}{50.883[1 - 1.7826I^2]} \tag{16}$$

where $I = (A\text{-}2Z)/A$ is the relative neutron excess of compound nucleus. The effective fissility parameter $x_{\text{eff,}}$ which includes the effect of mass and charge asymmetry, is as [37]

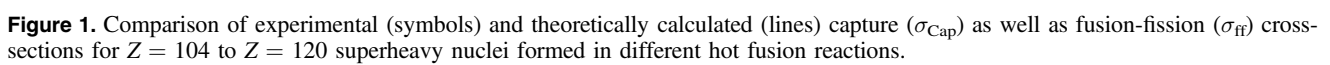$$x_{\text{eff}} = \frac{4Z_1Z_2/[A_1^{1/3}A_2^{1/3}(A_1^{1/3} + A_2^{1/3})]}{50.883[1 - 1.7826I^2]}. \tag{17}$$

The value of P_{CN}^0, which is the 'asymptotic' fusion probability, was proposed by Zagrebaev and Greiner [38]. It depends on the above parameters of the colliding nuclei by the relation

$$P_{\text{CN}}^0 = \frac{1}{1 + \exp(x_{\text{m}} - \xi)/\tau}. \tag{18}$$

The parameters of equation (18), giving better agreement with the estimated values of P_{CN}^0 for reactions with actinide targets, are defined as $\tau = 0.0226$ and $\xi = 0.721$ [36]. The energy dependence of fusion probability can be approximated by simple relation as [38]

$$P_{\text{CN}}(E^*, \ell) = \frac{P_{\text{CN}}^0}{1 + \exp[(E_B^* - E_{\text{CN}}^*)/\triangle]}. \tag{19}$$

Here E_B^* is the excitation energy of compound nucleus equal to bass barrier, E_{CN}^* is the excitation energy, and $\triangle$ is the adjustable parameter of about 4 MeV. Also, the Businaro-Gallone mass asymmetry (α_{BG}) is calculated using empirical

Figure 1. Comparison of experimental (symbols) and theoretically calculated (lines) capture (σ_{Cap}) as well as fusion-fission (σ_{ff}) cross-sections for $Z = 104$ to $Z = 120$ superheavy nuclei formed in different hot fusion reactions.

relation [39]

$$\alpha_{BG} = \begin{cases} 0; \ x_{CN} < 0.396 \\ 1.12\sqrt{\dfrac{x_{CN} - 0.396}{x_{CN} - 0.156}}; \ x_{CN} > 0.396 \end{cases}. \qquad (20)$$

3. Results and discussions

This section is divided into two subsections: section 3.1 and section 3.2. In section 3.1, the stratagem described above is applied to the analysis of experimental findings [18, 36, 40–43] over a wide range of superheavy nuclei. A comparison of formation cross-sections for $Z = 104$–120 superheavy elements and barrier characteristics is made at energies near and above the Coulomb barrier. Afterwards in section 3.2, the same methodology is used to evaluate the capture and fusion (or fusion-fission) excitation functions for ^{258,267,269,271}Bh, ^{267,271,273,275}Mt, ^{274,275,278,280}Ds, and ^{275,277,279}Rg nuclei. The projectile and target combinations are chosen in such a way that their half lives are significantly large. As mentioned in the introduction, the contribution of evaporation residue cross-sections, σ_{ER} (of the order of nb and pb) toward fusion is very small as compared to the fusion-fission cross-sections (of the order of mb), which means that $\sigma_{fusion} \sim \sigma_{ff}$ and hence the fusion cross-sections (σ_{fusion}) estimated using Wong criteria are termed as fusion-fission cross-sections (σ_{ff}). Beside this, an attempt is made to analyze the different factors effecting the quasi-fission and fusion-fission contributions.

3.1. Comparison of barrier characteristics and cross-sections with available data

Figure 1 shows the capture and fusion (equivalently fusion-fission) excitation functions of superheavy nuclei with $Z = 104$–120 at energies near and above the Coulomb barrier. The experimentally available capture (σ_{Cap}) and fusion-fission (σ_{ff}) cross-sections are compared with the theoretical estimates of the ℓ-sum Wong model. For the purpose, ^{26}Mg+^{238}U→^{264}Rf* [18], ^{27}Al+^{238}U→^{265}Db* [18], ^{30}Si+^{238}U→^{268}Sg* [40], ^{34}S+^{238}U→^{272}Hs* [41], ^{36}S+^{238}U→^{274}Hs* [42], ^{35}Cl+^{238}U→^{273}Mt* [18], ^{48}Ti+^{238}U→^{286}Fl* [36], ^{48}Ca+^{244}Pu→^{292}Fl* [43], ^{48}Ca+^{248}Cm→^{296}Lv* [43], and ^{64}Ni+^{238}U→^{302}120* [36] reactions are taken into account and variation of cross-sections with excitation energy (E_{CN}^*) is plotted in figure 1. This figure clearly illustrates that theoretically calculated cross-sections (denoted by lines) are in reasonable agrement with the available experimental data (denoted by filled symbols) for most of the cases. An important result that can be depicted from this figure is that the capture cross-sections (σ_{Cap}) for all the aforesaid reactions are in good agrement with the experimental data but there is some discrepancy in the fusion-fission cross-sections (σ_{ff}) for some reactions.

The σ_{Cap} as well as σ_{ff} data of ^{268}Sg*, ^{272}Hs*, ^{274}Hs*, ^{286}Cn*, ^{286}Fl*, ^{292}Fl*, ^{296}Lv*, and ^{302}120* superheavy nuclei is reproduced well (see figures 1(c)–(e), (g)–(k)). On the other
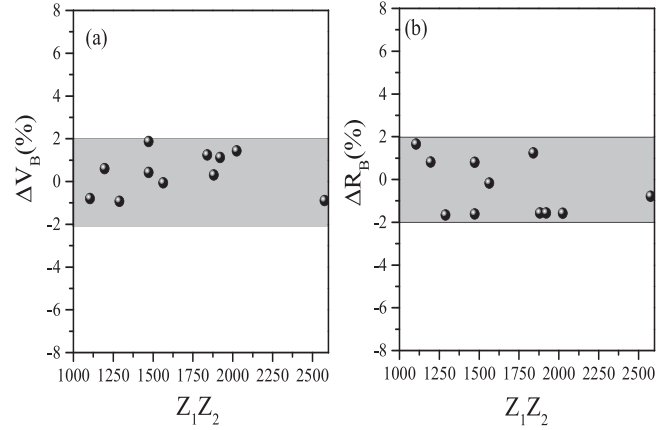

Figure 2. The percentage deviation of (a) barrier height (V_B) and barrier radius (R_B) from experimental numbers as a function of the charge product (Z_1Z_2) by taking deformations up to β_2 at 'optimum' orientations.

hand, for ^{264}Rf*, ^{265}Db*, and ^{273}Mt*, σ_{Cap} is fitted but σ_{ff} show deviation from experimental data. The σ_{ff} are over-estimated for ^{264}Rf* and ^{265}Db* superheavy nuclei and underestimated for the ^{273}Mt* system as shown in figures 1(a)–(b), and (f) respectively. It is relevant to mention here that, the experimental data available for these three systems is rather old [18] in comparison to other cases [36, 40–43]. The inconsistency in theoretically estimated fission cross-sections might be due to the anomaly in compound nuclear formation probability (P_{CN}) values calculated using equation (19).

The extensive comparative study of fusion barrier characteristics for colliding nuclei mentioned in figure 1 is also carried out. The barrier characteristics are estimated by taking β_2-deformations of nuclei with optimum orientations [44]. It may be noted that the position and height of the Coulomb barrier could not be measured directly in an experiment and the barrier characteristics mentioned in experimental work of [18, 36, 40–43] are close to the one calculated using the NRV code (link is provided in [21]). The percentage deviation of theoretical (ℓ-summed Wong model) and experimental Coulomb barrier height (V_B) and Coulomb barrier radius (R_B) are plotted in figure 2 as a function of charge product of incoming nuclei. The percentage deviation of Coulomb barrier height, ΔV_B (%) and Coulomb barrier radius, ΔR_B (%) is defined as

$$\Delta V_B(\%) = \frac{V_B^{Exp.} - V_B^{\ell}}{V_B^{Exp.}}; \ \Delta R_B(\%) = \frac{R_B^{Exp.} - R_B^{\ell}}{R_B^{Exp.}} \qquad (21)$$

The theoretically calculated barrier heights (V_B) and radius (R_B) are in good agrement with the experimental one. The calculated barrier parameters have an accuracy of ~98% and can be reproduced in an approximate deviation range of ±2%. Conclusively, one can say that the ℓ-summed Wong model reproduces the barrier characteristics and hence the cross-sections nicely and hence could be used to make some relevant predictions.

Table 1. ℓ-summed Wong calculated Coulomb barrier height (V_B), barrier position (R_B), along with deformations (β_{2i}), Coulomb factor ($Z_P Z_T$), Businaro-Gallone mass asymmetry (α_{BG}), entrance channel mass-asymmetry (η), |Q|-value of entrance channel for the synthesis of $Z = 107, 109, 110,$ and 111 superheavy nuclei.

Reaction	β_{2i}	$Z_P Z_T$	α_{BG}	η	R_B	V_B	$|Q|$
Z = 107							
^{48}Ti+^{210}At→^{258}Bh*	(0.00,0.00)	1870	0.927	0.628	12.60	202.56	172.60
^{48}Ca+^{223}Fr→^{271}Bh*	(0.00,0.132)	1740	0.922	0.646	13.00	181.60	151.83
^{36}S+^{231}Pa→^{267}Bh*	(0.00,0.195)	1456	0.924	0.730	12.60	155.30	116.00
^{31}P+^{238}U→^{269}Bh*	(−0.218,0.236)	1380	0.923	0.769	12.20	152.30	98.61
^{30}Si+^{237}Np→^{267}Bh*	(−0.236,0.226)	1302	0.924	0.775	12.20	143.50	98.30
^{24}Mg+^{243}Am→^{267}Bh*	(0.393,0.237)	1140	0.924	0.820	11.70	128.70	75.52
Z = 109							
^{48}Ti+^{223}Fr→^{271}Mt*	(0.00,0.132)	1914	0.929	0.645	12.90	199.90	161.20
^{48}Ca+^{227}Ac→^{275}Mt*	(0.00,0.164)	1780	0.927	0.651	13.00	186.12	157.00
^{36}S+^{237}Np→^{273}Mt*	(0.00,0.226)	1488	0.928	0.736	12.60	158.40	120.22
^{35}Cl+^{238}U→^{273}Mt*	(−0.234,0.236)	1380	0.928	0.743	12.30	171.10	116.20
^{30}Si+^{243}Am→^{273}Mt*	(−0.236,0.237)	1330	0.928	0.780	12.20	146.30	101.70
^{24}Mg+^{247}Bk→^{271}Mt*	(0.393,0.249)	1140	0.930	0.823	11.90	130.80	79.50
Z = 110							
^{48}Ti+^{226}Ra→^{274}Ds*	(0.00,0.164)	1936	0.931	0.649	12.90	202.20	163.90
^{48}Ca+^{232}Th→^{280}Ds*	(0.00,0.205)	1800	0.929	0.662	12.90	187.34	159.03
^{40}Ar+^{238}U→^{278}Ds*	(−0.031,0.236)	1656	0.930	0.712	11.90	179.10	134.07
^{36}S+^{242}Pu→^{278}Ds*	(0.00,0.237)	1504	0.930	0.741	12.60	159.50	122.20
^{30}Si+^{248}Cm→^{278}Ds*	(0.0,0.235)	1344	0.930	0.784	12.20	147.50	103.30
^{24}Mg+^{251}Cf→^{275}Ds*	(0.393,0.250)	1140	0.931	0.825	11.80	132.20	81.40
Z = 111							
^{48}Ti+^{227}Ac→^{275}Rg*	(0.00,0.164)	1958	0.934	0.651	12.80	204.80	167.90
^{48}Ca+^{231}Pa→^{279}Rg*	(0.00,0.195)	1820	0.932	0.656	12.90	190.00	162.30
^{39}K+^{238}U→^{277}Rg*	(−0.032,0.236)	1748	0.933	0.718	12.20	191.50	134.70
^{36}S+^{243}Am→^{279}Rg*	(0.00,0.237)	1520	0.932	0.742	12.60	161.80	125.00
^{30}Si+^{247}Bk→^{277}Rg*	(−0.236,0.249)	1358	0.933	0.783	12.20	149.20	107.10

3.2. Production of Z = 107 (Bh), 109 (Mt), 110 (Ds), and 111 (Rg) superheavy isotopes

After comparing the barrier characteristics and cross-sections with available experimental data, the ℓ-summed Wong model is applied to study the least explored superheavy nuclei i.e. $Z = 107, 109, 110,$ and 111. The main aim of the present work is to predict the capture and fusion-fission cross-sections for different isotopes of superheavy nuclei. For the purpose, various t-p combinations are taken into account as shown in table 1. The fusion barrier parameters (R_B, V_B) for the chosen reaction partners are tabulated in table 1 along with deformations ($\beta_{\lambda i}$), Coulomb factor ($Z_P Z_T$), critical Businaro-Gallone mass asymmetry (α_{BG}), entrance channel mass-asymmetry (η), and |Q|-value. In the case of superheavy nuclei, the chances of fusion are relatively less as compared to the lighter mass systems and it is hindered by quasi-fission (QF) events. Hence, all the above mentioned factors impart considerable significance in the estimation of fusion-fission cross-sections of superheavy nuclei.

The following observations can be withdrawn from table 1: (i) the Coulomb barrier height (V_B) decreases with the decrease in Coulomb factor ($Z_P Z_T$) and increase in mass-asymmetry (η). This ultimately effects the fusion (hence fission) cross-sections and these are expected to increase with an increase in η. (ii) The Coulomb factor ($Z_P Z_T$) is related to the

Coulomb repulsive energy in entrance channel and higher magnitude of Coulomb factor indicates the possible occurrence of quasi-fission (QF). According to the macroscopic-microscopic model [45], if $Z_P Z_T > 1600$, QF events are more prominent. In table 1, reactions are chosen in such a way that $Z_P Z_T$ of entrance channel lies across the aforesaid limit. The $Z_P Z_T$ for ^{48}Ti- and ^{48}Ca-induced reactions is above 1600 and the same for ^{24}Mg, ^{30}Si, and ^{36}S induced reactions is below this limit. This indicates that for more asymmetric reactions, there are higher chances of fusion. Also, with the increase in charge number (Z), the Coulomb factor ($Z_P Z_T$) for most of the reactions start approaching this threshold value. Conclusively, the symmetric interacting pairs generally lead to significant contribution of QF components. (iii) In asymmetric combinations of colliding nuclei, fusion suppression can also be observed by an effect of the conditional barrier. So, for the case, Businaro-Gallone mass asymmetry point (α_{BG}) define the fusion process. Systems having $\eta \sim \alpha_{BG}$, there are higher chances of fusion. In contrast, for $\eta < \alpha_{BG}$, it is expected that fusion is not complete and there are chances of QF. For the reaction pairs mentioned in table 1, $\eta < \alpha_{BG}$ and it is expected that QF appears in the company of fusion-fission processes. The contribution of QF may be different for different channels depending on the deviation of η from α_{BG} and some other related factors.
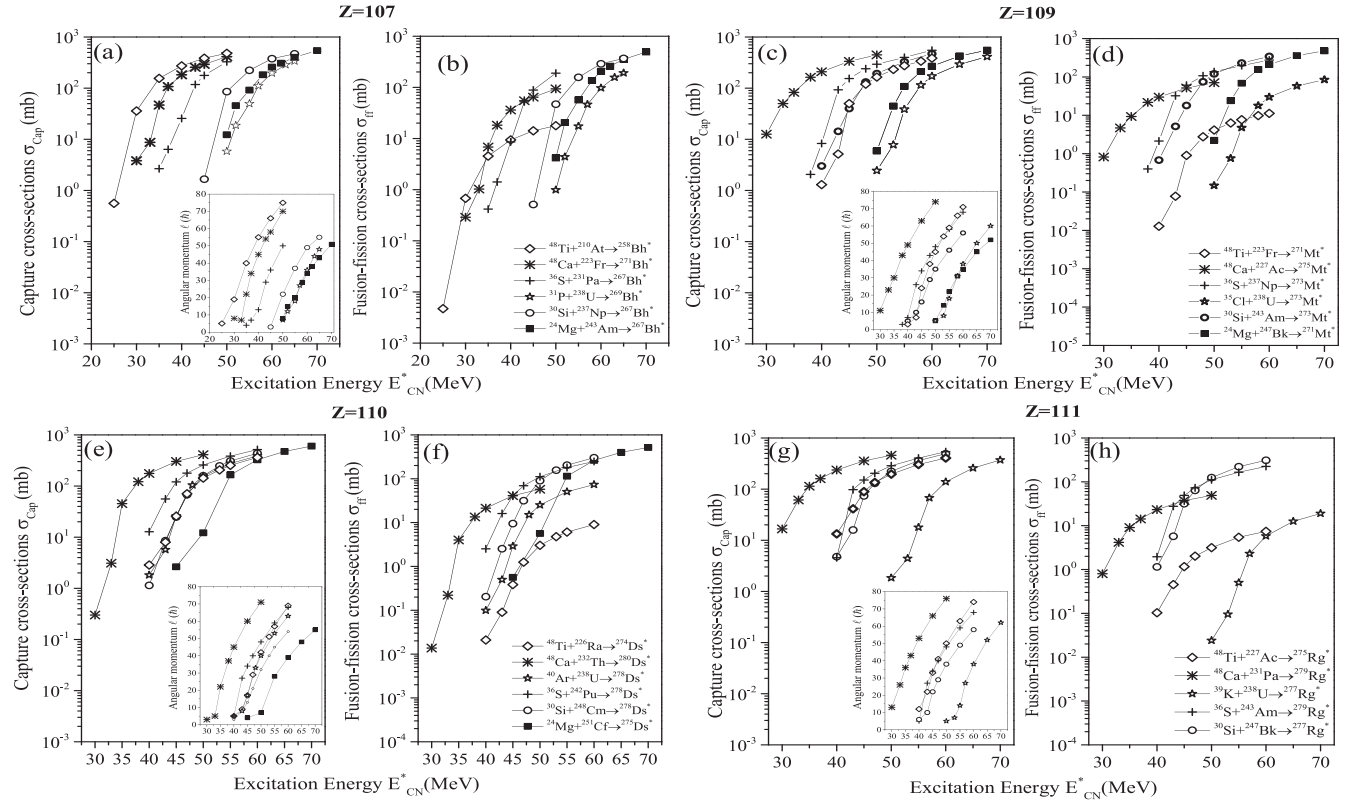
Figure 3. Theoretically predicted capture (σ_{Cap}) and fusion-fission (σ_{ff}) excitation functions for the synthesis of (a), (b) $Z = 107$, (c), (d) $Z = 109$, (e), (f) $Z = 110$, and (g), (h) $Z = 111$ superheavy nuclei. The respective ℓ-values are also shown in the inset of figures.
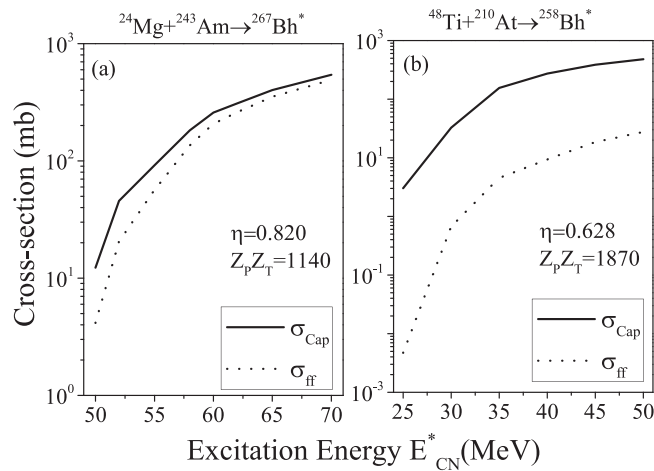

Figure 4. Variation of capture and fusion-fission cross-sections for $Z = 107$ as a function of excitation energy (E_{CN}^*) for (a) ^{24}Mg+^{243}Am (b) ^{48}Ti+^{210}At reactions.

The theoretically calculated capture (σ_{Cap}) and fusion-fission (σ_{ff}) excitation functions for the reaction partners mentioned in table 1 are plotted in figure 3 for near and above barrier energies. Figures 3(a), (c), (e), (g) represent the capture and figures 3(b), (d), (f), (h) show the fusion-fission cross-sections as a function of excitation energy (E_{CN}^*). The respective angular momentum values (ℓ_{max}) are plotted in the inset as a function of excitation energy (E_{CN}^*). It is evident from this figure that the variation of cross-sections is smooth

with excitation energy. The cross-section increases with increase in energy and then start saturating. An important observation that can be noticed from this figure is that the magnitude of capture cross-sections (σ_{Cap}) for the chosen reactions are quite close to each other. The comparison of σ_{Cap} at energies close to the Coulomb barrier shows that the ratio of cross-section values for reactions with lowest mass-asymmetry to highest mass asymmetry (i.e. $\sigma_{Cap}^{\eta_{\text{lowest}}}/\sigma_{Cap}^{\eta_{\text{highest}}}$) is $\approx$1–2. In contrast to above, the fusion-fission cross-sections are evidently different for the reactions under consideration. Higher fusion-fission cross-sections are observed for super-heavy nuclei formed in ^{24}Mg-induced reactions followed by ^{30}Si and ^{36}S. The observed fission cross-sections are nearly identical for ^{30}Si and ^{36}S projectiles for most of the cases. Although the cross-sections are obtained higher with ^{24}Mg, ^{36}S can still be a preferable choice due to relatively lower excitation energies. Also, the reactions with a doubly magic ^{48}Ca projectile have sufficiently values with lower excitation energies, which can be a good alternative for the synthesis of such nuclei. It can be used for the synthesis of neutron rich isotopes of respective nuclei. The least cross-sections are observed for the use of ^{48}Ti-induced reactions.

Figure 4 is plotted to analyze the contribution of quasi-fission process towards capture cross-sections. The variation of σ_{Cap} and σ_{ff} is plotted as a function of excitation energy (E_{CN}^*) for two extreme mass-asymmetric reaction pairs leading to the formation of $Z = 107$ (Bh) superheavy isotopes. Larger capture and fusion-fission cross-sections are observed for ^{24}Mg+^{243}Am$\rightarrow^{267}$Bh* reaction as compared to
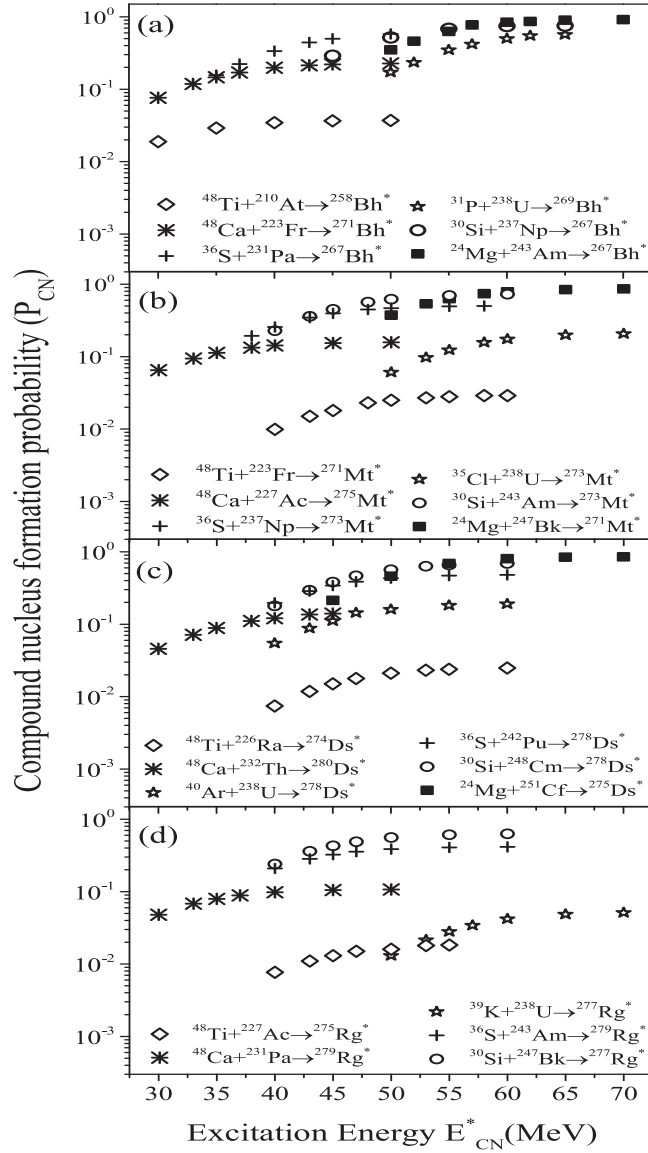
Figure 5. Compound nucleus formation probabilities (P_{CN}) plotted as a function of excitation energy (E^*_{CN}) for $Z = 107$, 109, 110, and 111 superheavy nuclei formed via different entrance channels.

Figure 6. Variation of capture cross-section at each target angle (θ_T) for ^{24}Mg+^{243}Am reaction at energy near the Coulomb barrier ($E^*_{CN} = 52$ MeV).

Figure 7. Variation of fission barrier heights (B_f) and neutron separation energy (B_n) as a function of compound nucleus fissility parameter (x_{CN}) for $Z = 107$, 109, 110, and 111 superheavy nuclei.

^{48}Ti+^{210}At→^{258}Bh*. The difference between capture and fusion-fission cross-sections is significantly large for ^{48}Ti-induced reaction and is observed least for the use of ^{24}Mg-projectile. For energies near the Coulomb barrier, the difference is larger as compared to the above barrier region. This deviation between cross-sections indicate the contribution of QF processes. Hence one can say that the quasi-fission events are more pronounced for ^{48}Ti-projectiles compared to others, which in turn further justify the above points. Similar types of results are observed for $Z = 109$, 110, and 111 superheavy nuclei, which are not shown here to avoid repetition. This difference in σ_{Cap} and σ_{ff} is evidently caused by the corresponding change in the compound nucleus formation probability (P_{CN}) value.

As mentioned in section 2, equation (19) determines the compound nucleus formation probability (P_{CN}) for the reactions leading to the formation of heavy/superheavy nuclei.
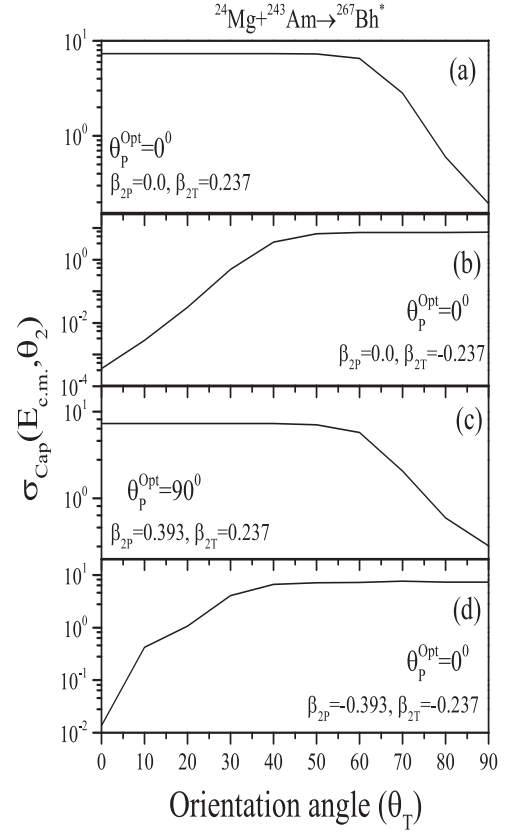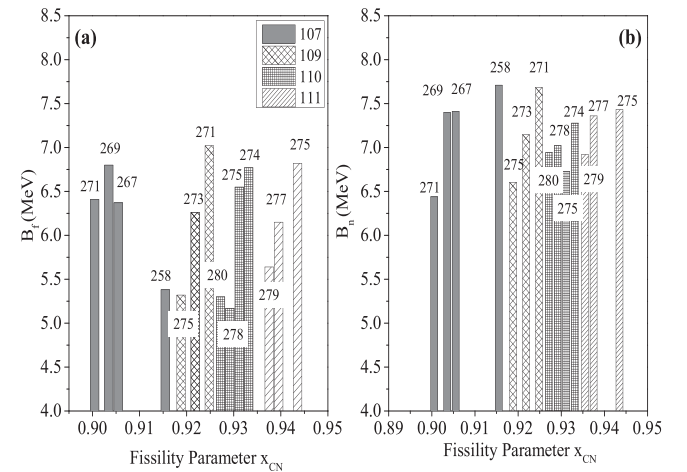
The calculated P_{CN} for different incoming channels are plotted in figure 5. P_{CN} is the measure of fusion suppression effects correlated with the entrance channel mass-asymmetry (η). Variation of P_{CN} is smooth and increases exponentially with the increase in excitation energy (E^*_{CN}). It becomes nearly constant at higher energies. Figure 5(a) shows that, out of all the reactions under consideration for the synthesis of $Z = 107$, the P_{CN} values are observed higher and comparable

Table 2. Survival probability of 3n and 4n evaporation channel (W_{Surv}^{3n} and W_{Surv}^{4n}) calculated using relation $W_{Surv} = \frac{\sigma_{ER}}{\sigma_{ER} + \sigma_{ff}}$ by considering present calculations and evaporation data of [22].

E_{CN}^* (MeV)	σ_{3n} (pb)	σ_{4n} (pb)	σ_{ff} (mb)	W_{Surv}^{3n}	W_{Surv}^{4n}
		^{36}S+^{237}Np→^{273}Mt*			
38		0.78	0.399		1.95×10^{-9}
40		3.12	2.13		1.45×10^{-9}
43		6.29	32.2		1.95×10^{-10}
45		5.38	60.8		8.84×10^{-11}
50		1.05	137.2		7.65×10^{-12}
		^{36}S+^{242}Pu→^{278}Ds*			
40	0.144	0.66	2.52	5.70×10^{-11}	2.60×10^{-10}
43	0.089	0.96	16.07	4.97×10^{-12}	5.90×10^{-11}
45	0.046	0.79	41.25	1.15×10^{-12}	1.90×10^{-11}
47	0.019	0.47	69.31	2.70×10^{-13}	6.78×10^{-12}
50	—	0.16	111.62	—	1.43×10^{-12}
		^{36}S+^{243}Am→^{279}Rg*			
40	0.813	2.36	0.95	8.53×10^{-10}	8.70×10^{-10}
43	0.266	2.24	27.70	9.60×10^{-12}	8.8×10^{-11}
45	0.109	1.31	49.04	2.20×10^{-12}	2.6×10^{-11}
47	—	0.65	72.83	—	8.9×10^{-12}
50	—	0.20	111.18	—	1.8×10^{-12}

for ^{24}Mg+^{243}Am and ^{30}Si+^{237}Np reactions followed by ^{36}S+^{231}Pa. In contrast, the least values are observed for ^{48}Ti+^{210}At. For $Z = 109$ (see figure 5(b)), $Z = 110$ (see figure 5(c)), and $Z = 111$ (see figure 5(d)), the formation probability of ^{36}S and ^{30}Si induced reactions are comparable. A drastic difference in the formation probability is observed for the interaction with ^{48}Ca and ^{48}Ti projectiles. The Coulomb barrier is larger and mass-asymmetry is lesser for the latter case. Hence lower P_{CN} values are observed for ^{48}Ti, which in turn result in stronger fusion hindrance as compared to the ^{48}Ca projectile.

The respective orientations of the interacting nuclei also play an important role and effect the cross-section contribution significantly. The same is explored via figure 6 which shows the variation of capture cross-sections (σ_{Cap}) at different orientation angles for ^{24}Mg+^{243}Am→^{267}Bh* reaction. Figures 6(a)–(d) are plotted respectively for spherical+prolate, spherical+oblate, prolate+prolate, and oblate+oblate choices of interacting nuclei. The projectile angle (θ_P) is kept fixed at optimum orientation [44] and target angle (θ_T) is varied. It is observed that the capture cross-section is maximum at $\theta_T = 0^0$ for prolate and $\theta_T = 90^0$ for oblate nuclei. Also, the observed σ_{Cap} are slightly higher for the deformed choice of nuclei relative to spherical+spherical (not shown here) and spherical +deformed pairs. This is possibly due to the fact that the deformation and orientation of nuclei change the balance between repulsive and attractive forces, which ultimately effect the Coulomb barrier and hence the cross-sections.

Figure 7 shows the variation of fission barrier heights (B_f) and neutron separation energy (B_n) with a compound nucleus fissility parameter (x_{CN}). Experimental nuclear masses [46] are used for the determination of neutron separation energies (B_n). The Möller and Nix masses of [47] are used where the experimental data is not available. It is relevant to mention

that the theoretical estimations of fission barrier for superheavy nuclei are not yet very reliable and differ significantly for different choices of methodologies, therefore systematic study of such quantities is highly desirable. It is evident from this figure that, with the increase in proton number Z of nuclei, the compound nucleus fissility parameter (x_{CN}) increases. Higher values of x_{CN} suggest the higher chances of separation of a compound nucleus. Also, with the increment in the mass of the superheavy isotopes, the fission barrier (B_f) decreases for most of the cases under consideration (see figure 7(a)). However, some uncertainty is observed for ^{269}Bh*, which is possibly due to the appearance of deformed neutron magic (N=162). The neutron separation energy (B_n) is plotted as a function of x_{CN} in figure 7(b). The magnitude of B_n is relatively higher as compared to B_f for most of the cases, which in turn suggests that fission is more prominent than the neutron evaporation process. The evaporation residue study of ^{36}S-induced reactions for $Z = 109$–111 was performed in [22] so using the evaporation residue data from [22] and fusion-fission cross-sections from present calculations, the survival probabilities (W_{Surv}) are calculated and mentioned in table 2. The W_{Surv} is calculated using relation $W_{Surv} = \frac{\sigma_{ER}}{\sigma_{ER} + \sigma_{ff}}$ [43]. This table shows that for a given compound system, the survival probability decreases with the increase in excitation energy (E_{CN}^*). Also, for given energies, the survival probability of 4n channel is higher as compared to that of 3n.

4. Summary

A systematic analysis of barrier characteristics, capture and fusion-fission cross-sections is carried out at near and above

the Coulomb barrier energies using the ℓ-summed Wong methodology and the experimental data is adequately addressed for $104 \leqslant Z \leqslant 120$ nuclei. Further, this approach is implemented to the estimations of capture and fission excitation functions for the isotopes of ^{258,267,269,271}Bh, ^{267,271,273,275}Mt, ^{274,275,278,280}Ds, and ^{275,277,279}Rg nuclei. It has been observed that the mass-asymmetric reactions involving ^{24}Mg, ^{30}Si, and ^{36}S projectiles seem more suitable to synthesize the above-mentioned superheavy isotopes. But due to lower excitation energy and higher cross-sections, ^{36}S can gain much attention. Beside this, the doubly magic ^{48}Ca provides an alternativee option for the synthesis of neutron rich isotopes which result in enhanced cross-sections in comparison to the ^{48}Ti projectile. Finally, an effort is made to analyze the relative contribution of fusion-fission and quasi-fission components. With the increase in Z-number and hence Coulomb factor ($Z_P Z_T$), the deviation of η from α_{BG} increases, which indicates the enhanced contribution of QF events. For a given Z, the magnitude of capture cross-section is nearly the same, whereas the σ_{ff} varies, significantly suggesting different involvement of the QF component. The deformations and orientations also play an important role in the determination of cross-sections. The cross-section values enhance with the addition of deformations as compared to the spherical case.

Acknowledgments

References

[1] Hofmann S 1997 *Nucl. Instrum. Methods. Phys. Res.* B **126** 310–5
[2] Hofmann S 1999 *Nucl. Phys.* A **654** 252c–269c
[3] Oganessian Y T 1975 *Nucl. Phys.* A **239** 353–64
[4] Oganessian Y T 2007 *J. Phys. G: Nucl. Part. Phys.* **34** R165–242
[5] Oganessian Y T *et al* 2004 *Phys. Rev.* C **70** 064609
[6] Oganessian Y T *et al* 2013 *Phys. Rev.* C **87** 014302
[7] Nelson S L *et al* 2008 *Phys. Rev.* C **78** 024606
[8] Hofmann S *et al* 1997 *Z. Phys.* A **358** 377–8
[9] Nelson S L *et al* 2009 *Phys. Rev.* C **79** 027605
[10] Folden C M *et al* 2004 *Phys. Rev. Lett.* **93** 212702
[11] Morita K *et al* 2004 *J. Phys. Soc. Jpn.* **73** 1738–44
[12] Morita K *et al* 2007 *J. Phys. Soc. Jpn.* **76** 043201
[13] Dvorak J *et al* 2006 *Phys. Rev. Lett.* **97** 242501
Dvorak J *et al* 2008 *Phys. Rev. Lett.* **100** 132503
[14] Graeger R *et al* 2010 *Phys. Rev.* C **81** 061601(R)
[15] Oganessian Y T *et al* 2013 *Phys. Rev.* C **87** 034605
[16] Toke J *et al* 1985 *Nucl. Phys.* A **440** 327
[17] Back B B *et al* 1981 *Phys. Rev. Lett.* **46** 1068–71
[18] Shen W Q *et al* 1987 *Phys. Rev.* C **36** 115–42
[19] Adamian G G *et al* 1998 *Nucl. Phys.* A **633** 409–20
[20] Cherepanov E A 2004 *Nucl. Phys.* A **734** E13–6
[21] Itkis M G *et al* 2015 *Nucl. Phys.* A **944** 204–37
[22] Hong J, Adamian G G and Antonenko N V 2016 *Eur. Phys. J.* A **52** 305
[23] Mayers W D *et al* 2000 *Phys. Rev.* C **62** 044610
[24] Zagrebaev V I 2004 *Nucl. Phys.* A **734** 164
[25] Dutt I and Puri R K 2010 *Phys. Rev.* C **81** 044615
[26] Denisov V Y 2002 *Phys. Lett.* B **526** 315–21
[27] Blocki J *et al* 1977 *Ann. Phys. (N. Y.)* **105** 427–62
[28] Gupta R K, Singh N and Manhas M 2004 *Phys. Rev.* C **70** 034608
[29] Wong C Y *et al* 1973 *Phys. Rev. Lett.* **31** 766–9
[30] Alder K and Winther A 1969 *Nucl. Phys.* A **132** 1–4
[31] Hill D L and Wheeler J A 1953 *Phys. Rev.* **89** 1102
Thomas T D 1959 *Phys. Rev.* **116** 703
[32] Miller S C and Good R H 1953 *Phys. Rev.* **91** 174–9
[33] Jain D *et al* 2014 *Eur. Phys. J.* A **50** 155
[34] Kumar R *et al* 2009 *Phys. Rev.* C **80** 034618
[35] Gull M *et al* 2018 *Phys. Rev.* C **98** 034603
[36] Kozulin E M *et al* 2016 *Phys. Rev.* C **94** 054613
[37] du Rietz R *et al* 2013 *Phys. Rev.* C **88** 054618
[38] Zagrebaev V I and Greiner W 2015 *Nucl. Phys.* A **944** 257
Zagrebaev V I and Greiner W 2008 *Phys. Rev.* C **78** 034610
[39] Saxena A *et al* 1994 *Phys. Rev.* C **49** 932–40
[40] Nisho K *et al* 2010 *Phys. Rev.* C **82** 044604
[41] Nisho K *et al* 2010 *Phys. Rev.* C **82** 024611
[42] Itkis M G *et al* 2010 *Nucl. Phys.* A **834** 374–7
[43] Kozulin E M *et al* 2014 *Phys. Rev.* C **90** 054608
[44] Gupta R K *et al* 2005 *J. Phys. G: Nucl. Part. Phys.* **31** 631–44
[45] Swiatecki W J 1981 *Phys. Scr.* **24** 113
[46] Wang M 2012 *Chin. Phys.* C **36** 1603–2014
[47] Moller P 2016 *At. Data Nucl. Data tables* **109–110** 1–204